Strategies to improve the explanatory power of a dynamic slope stability model by enhancing land cover parameterisation and model complexity

Schmaltz, Elmar M.; Van Beek, L. P.H.; Bogaard, Thom A.; Kraushaar, Sabine; Steger, Stefan; Glade, Thomas

DOI
10.1002/esp.4570

Publication date
2019

Document Version
Final published version

Published in
Earth Surface Processes and Landforms

Citation (APA)
Schmaltz, E. M., Van Beek, L. P. H., Bogaard, T. A., Kraushaar, S., Steger, S., & Glade, T. (2019). Strategies to improve the explanatory power of a dynamic slope stability model by enhancing land cover parameterisation and model complexity. *Earth Surface Processes and Landforms*, *44*(6), 1259-1273. https://doi.org/10.1002/esp.4570

EARTH SURFACE PROCESSES AND LANDFORMS
Earth Surf. Process. Landforms (2019)

Published online in Wiley Online Library
(wileyonlinelibrary.com) DOI: 10.1002/esp.4570

Strategies to improve the explanatory power of a dynamic slope stability model by enhancing land cover parameterisation and model complexity

Elmar M. Schmaltz,[1,2]* L.P.H. Van Beek,[3] Thom A. Bogaard,[4] Sabine Kraushaar,[2] Stefan Steger[5] and Thomas Glade[2]
[1] Federal Agency for Water Management, Institute for Land and Water Management Research, Pollnbergstraße 1, 3252 Petzenkirchen, Austria
[2] ENGAGE – Geomorphological Systems and Risk Research, Faculty of Earth Sciences, Geography and Astronomy, University of Vienna, Austria
[3] Department of Physical Geography, Utrecht University, PO Box 80115, 3508 TC Utrecht, The Netherlands
[4] Water Resources Section, Delft University of Technology, Stevinweg 1, 2628 CN Delft, The Netherlands
[5] EURAC Research, Institute for Earth Observation, Drususallee 1, 39100 Bozen/Bolzano, Italy

Received 2 March 2018; Revised 3 December 2018; Accepted 6 December 2018

*Correspondence to: Elmar M. Schmaltz, Federal Agency for Water Management, Institute for Land and Water Management Research, Pollnbergstraße 1, 3252 Petzenkirchen, Austria. E-mail: elmar.schmaltz@baw.at

ESPL
Earth Surface Processes and Landforms

ABSTRACT: Despite the importance of land cover on landscape hydrology and slope stability, the representation of land cover dynamics in physically based models and their associated ecohydrological effects on slope stability is rather scarce. In this study, we assess the impact of different levels of complexity in land cover parameterisation on the explanatory power of a dynamic and process-based spatial slope stability model. Firstly, we present available and collected data sets and account for the stepwise parameterisation of the model. Secondly, we present approaches to simulate land cover: 1) a grassland landscape without forest coverage; 2) spatially static forest conditions, in which we assume limited knowledge about forest composition; 3) more detailed information of forested areas based on the computation of leaf area development and the implementation of vegetation-related processes; 4) similar to the third approach but with the additional consideration of the spatial expansion and vertical growth of vegetation. Lastly, the model is calibrated based on meteorological data sets and groundwater measurements. The model results are quantitatively validated for two landslide-triggering events that occurred in Western Austria. Predictive performances are estimated using the Area Under the receiver operating characteristic Curve (AUC). Our findings indicate that the performance of the slope stability model was strongly determined by model complexity and land cover parameterisation. The implementation of leaf area development and land cover dynamics further yield an acceptable predictive performance (AUC ~0.71-0.75) and a better conservativeness of the predicted unstable areas (FoC ~0.71). The consideration of dynamic land cover expansion provided better performances than the solely consideration of leaf area development. The results of this study highlight that an increase of effort in the land cover parameterisation of a dynamic slope stability model can increase the explanatory power of the model. © 2018 The Authors. Earth Surface Processes and Landforms published by John Wiley & Sons Ltd.

KEYWORDS: Shallow translational landslides; land cover dynamics; parameterisation; physically based slope stability modelling; STARWARS/PROBSTAB; predictive performance

Introduction

Landslides are regulating mechanisms that enable hillslope landscapes to adapt to changing conditions of mechanical stability. In many regions, landslide dynamics plays a key role in land transformation (Crozier 2010; Korup *et al.*, 2010; Glade and Crozier, 2005) and describes the coherent displacement of rock or soil over a discrete sliding surface (Van Beek, 2002) that can be triggered by transient extrinsic phenomena, such as heavy rainfalls or earthquakes (Crozier, 1986; Dikau *et al.*, 1996; Guzzetti *et al.*, 1999; Crozier and Glade, 1999). It is also suggested, that future changes of land use and land cover might highly influence landslide initiation and activity (Glade, 2003; Promper *et al.*, 2014; Malek *et al.*, 2015). In forested landscapes, particularly shallow slope failures of the slide-type (Cruden and Varnes, 1996), depict one of the dominant geomorphic hillslope processes that contribute to landscape shaping (Jakob *et al.*, 2005; Sidle and Ochiai, 2006; Papathoma-Köhle and Glade, 2013). Studies provide evidence that the forest cover of a hillslope landscape is generally able to reduce the frequency of shallow landslide occurrences (Glade, 2003; Sidle *et al.*, 2006; Ghestem *et al.*, 2011; Sidle and Bogaard, 2016).

Mechanical and hydrological effects define the influence of forests on slope stability and have both beneficial and adverse effects on the reinforcement of a slope (Sidle and Bogaard, 2016). O'Loughlin (1974) postulates that the stabilising effects of forests on slope stability outweigh the adverse effects. Along with O'Loughlin (1974), various pioneer studies investigated the impact of clear-cutting on slope stability and evinced the role of forests to counteract the landslide triggering mechanisms and to reduce the frequency of landslide occurrences (Endo and Tsuruta, 1969; O'Loughlin, 1974; Burroughs and Thomas 1977; Gray and Megahan, 1981; Ziemer 1981). Forests influence the hydrological balance of a hillslope considerably (Meng *et al.*, 2014; Sidle and Bogaard, 2016). Interception of tree canopies deters considerable amounts of precipitation and prevents intercepted water to infiltrate the soil. Transpiration leads to a reduction of the soil water content and depresses the groundwater table (Meng *et al.*, 2014), however, is mainly effective during dry season (Sidle and Ochiai, 2006) or even negligible where it considerably falls below the amount of precipitation (Gray and Sortir, 1996). Both effects strongly depend on seasonal climatic conditions (Watson *et al.*, 1999), but enable forests to contribute to a long-term reinforcement of hillslopes (O'Loughlin, 1974; Greenway, 1987; Sidle and Ochiai, 2006; Ghestem *et al.*, 2011). On the other hand, preferential flow of infiltrated water along root channels might accelerate the time to saturation of potentially critical soil layers, whereas increased root moisture content decrease the tensile strength of the roots (Hales and Miniat, 2017). Mechanically, trees provide stability by reinforcing the underlying soil mantle with a network of roots and thus protect the soil package from failure or prolong the time to the failing point, especially during landslide-triggering rainstorms (Greenway, 1987; Sidle and Ochiai, 2006; Papathoma-Köhle and Glade, 2013). Tree root systems provide mechanical stability even after forest removal but their reinforcement potential decrease after time, leading to a minimum of potential stabilisation between 3 and 8 years (O'Loughlin, 1974; Sidle *et al.*, 1985; Sidle 1992). However, there are mechanical-related properties of forests that might counteract the stabilisation of a slope, such as soil loosening by wind load or surcharge (Sidle and Ochiai, 2006; Ghestem *et al.*, 2011; Sidle and Bogaard, 2016). From a spatial perspective, the effects of forest cover are strongly dependent on the scale on which slope stability is assessed. At the hillslope scale, hydrological effects are presumably rather inferior compared to the biomechanical effects (Sidle and Ziegler, 2017; Cohen and Schwarz, 2017). In contrast, the impact of forest on the landscape hydrology at catchment or regional scale are remarkably higher when slopes drain large areas (Keim and Skaugset, 2003; Cohen and Schwarz, 2017) and might outrank the biomechanical effects. Hence, the spatio-temporal impact of forest has to be considered when assessing slope stability at regional scale on long-term periods, such as years or decades. The majority of the beforementioned hydrological processes and mechanical properties are directly or indirectly related to the apparent leaf area of the vegetation (Wilson, 1988). The leaf area determines the amount of potentially intercepted or stored water in the tree canopies, and thus prevents the infiltration of a critical amount of water into the soil (Ghestem *et al.*, 2011). Additionally, leaves control the amount of potential water that can be assimilated from the soil matrix. In this regard, photosynthetically active biomass governs the development of root mass that stabilises the plant and satisfies the water and nutrient demand. Consequently, it can be assumed that the leaf biomass indirectly controls the development and distribution of the plant roots and the potential of mechanical stability that can be provided by the root system (cf. studies of Hales *et al.* 2009, Meng *et al.*, 2018 and Zhou *et al.*, 2018). Hence, the parameterisation of the seasonal dynamics of leaf development is required to account for the impacts of biomass in physically slope stability models.

A set of spatially distributed and physically based slope stability models are available to simulate shallow translational slope instabilities applicable at different scales (Glade and Crozier 2005). Firstly proposed by Burroughs (1985), physically based models evolved that analyse the equilibrium of a soil-mantled slope under the gravitational force, e.g. static models such as SHALSTAB (Montgomery and Dietrich, 1994), SINMAP (Pack *et al.*, 1998), SHETRAN (Ewen *et al.*, 2000) or dynamic models such as TRIGRS (Baum *et al.*, 2002), STARWARS/PROBSTAB (Van Beek, 2002), GEOtop-FS (Simoni *et al.*, 2008) and HIRESSS (Rossi *et al.*, 2013). Recent research advances explicitly include the hydrological and mechanical influences of land cover into their innovative modelling approaches, such as MD-STAB (Milledge *et al.*, 2014; Bellugi *et al.*, 2015) and PRIMULA (Cislaghi *et al.*, 2018). The dynamic models mentioned above contain a hydrology component, however, differ very much concerning the opportunity for the user to change the parameterisation (Kuriakose *et al.*, 2009). In addition, only few of these models are able to account for hydrological and mechanical effects of vegetation on slope stability. Indeed, previous studies elucidated that the inclusion of a landscape's vegetation cover is crucial for the assessment of spatio-temporal slope stability in dynamic, process-based models (Vanacker *et al.*, 2003; Kuriakose *et al.*, 2009). However, the absence of reliable land cover maps carrying information on different forest types, stand densities and the apparent ages of stands or trees often hampers an accurate representation of the actual vegetation cover.

Previous research that accounted for land cover impacts on slope stability mainly focussed on biomechanical effects (Schwarz *et al.*, 2010; Wu *et al.*, 2013; Hales and Miniat, 2017). Other studies analysed (e.g. Chirico *et al.*, 2013; Arnone *et al.*, 2016; Kim *et al.*, 2017) or modelled (e.g. Band *et al.*, 2012; Hwang *et al.*, 2015) long-term hydrological effects of land cover on slope stability. However, the dynamic representation of leaf area development and associated inter-annual ecohydrological effects on the variability of slope stability in physically based models is rather scarce (Meng *et al.*, 2014; Sidle and Bogaard, 2016; Kim *et al.*, 2017) and requires more attention in dynamic slope stability modelling. In this study, we apply four land cover scenarios, with different representations of vegetation parameter input, annual leaf area development and land cover dynamics, to STARWARS/PROBSTAB (Van Beek, 2002) that couples a dynamic, hydrological component with a probabilistic geomechanical component. In doing so, we test the hypothesis that an increase of model complexity in the representation of vegetation-related dynamics and processes by land cover properties enhance the predictive performance of dynamic models applied for multi-annual time scales.

Study area

The 'Dreiklang region' is situated in the quaternary basin of the Walgau in Vorarlberg, Austria. Our study area is the south-facing hillside of the Northern ridge of the basin ('Walserkamm') that encloses the three villages Schnifis, Düns and Dünserberg (Montanast) with a size of approx. 12 km^2 and an elevation ranging from 625 to 1971 m.a.s.l. (cf. Figure 1A). Geologically, the basin is composed of sandstone formations (Fr and Fp) and calcareous Piesenkopf-formation (pi) of the Cretaceous Vorarlbergian Flysch (Oberhauser, 1972; Walach and Weber, 1977), overlain by quaternary

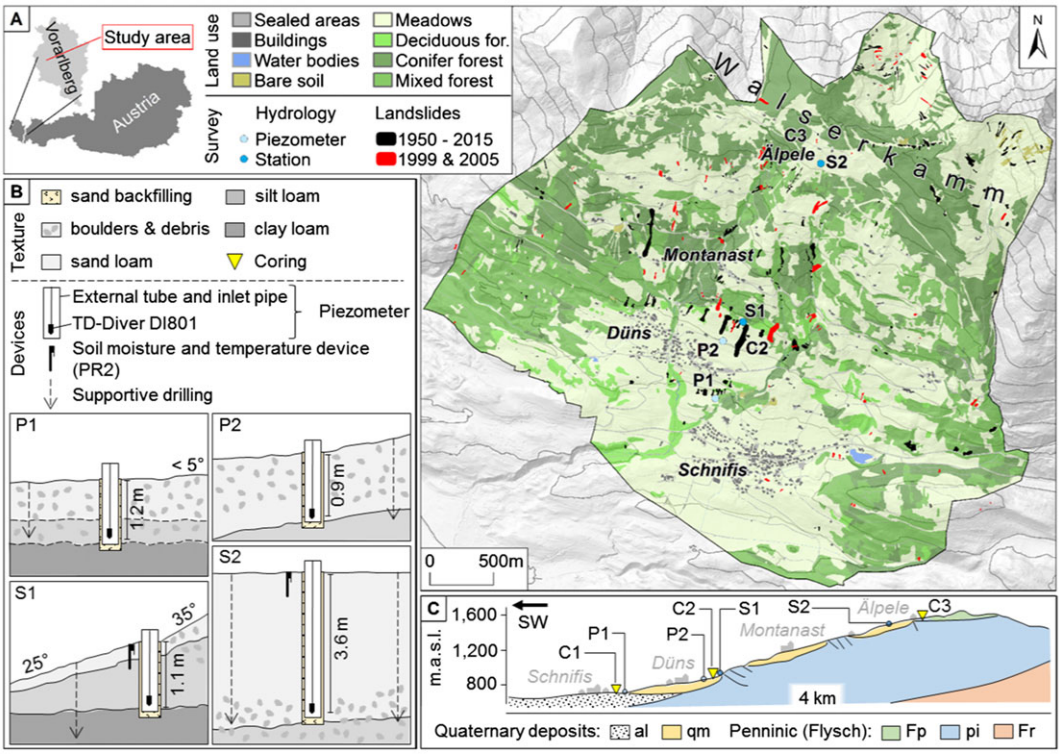

Figure 1. A: Localisation, land cover conditions in 2001 and shallow translational landslides (black: all mapped landslides from 1950 to 2015; red: landslides that were triggered after the extreme events of 1999 and 2005) of the Dreiklang region, including the positions of piezometers (P), meteorological stations (S) and corings (C). B: Cross-profiles show the arrangement of differently composed soil layers in adjacent areas of the respective P and S locations. C: Transect along the hillslope from SW to NE direction with the underlying geological formations, settlements and locations of P, S and C. [Colour figure can be viewed at wileyonlinelibrary.com]

morainic (qm) right up to the Walserkamm ridge (Loacker, 1971) and alluvial (al) deposits (Heissel *et al.*, 1967; Friebe, 2004; Ruff and Czurda, 2008; Seijmonsbergen *et al.*, 2014; Steger *et al.*, 2018). According to the Digital Soil Map of Austria (eBod), provided by the Federal Research and Training Centre for Forests, Natural Hazards and Landscape (BFW), mainly calcareous cambisols developed on the morainic and hillslope deposits, with few sprinkled locations of hillslope gley soils or fen areas. Soils in forested areas of the Dreiklang region are not considered in the eBod. Information about spatial composition and diversity of the soils in the study area very sparse, with only three recorded profiles for the research area. The regional agro-economy is primarily based on alpine pastures, with dairy cattle farming and timber harvesting of the largely distributed spruce and fir stands. In general, the total forested area increased by 12% from 630 ha in the 1980s to 678 ha in 2015 (Schmaltz *et al.*, 2017), exhibiting a remarkable change of forest and agricultural management in the region. Multiple investigations revealed high landslide dynamics in the Vorarlbergian Flysch Zone (Tilch, 2014; Zieher *et al.*, 2016), particularly in the Walgau valley (Seijmonsbergen, 1992; Seijmonsbergen *et al.*, 2014; Steger *et al.*, 2018) and in the Dreiklang region (Markart *et al.*, 2007; Schmaltz *et al.*, 2017). The landslide-triggering rainstorm events of May 1999 (64 landslides) and August 2005 (56 landslides) posed severe threats on infrastructure in the study area (Markart *et al.*, 2007). The event in 1999 started with a heavy, short-term rainfall of 251 mm on May 22, followed by an extraordinary snow intensive winter and a rapid snowmelt period. In 2005 a prolonged rainfall period with constant precipitation of 6 days with an average daily mean precipitation of 59 mm and a peak rainfall of approx. 164 mm day^{-1} on August 23.

Land cover parameterisation

In order to derive relevant vegetation parameters, a particular focus was set on the representation of the leaf area. We used an approach by Sellers *et al.* (1996) and Los *et al.* (2000) to calculate the Leaf Area Index (LAI) from the Normalised Differenced Vegetation Index (NDVI; Rouse *et al.*, 1973), based on aerial photographs from 2001 and 2011. A light transmittance reduction function (Bresinsky *et al.*, 2008) in combination with the calculated LAI-values and species-specific growth functions (Houllier *et al.*, 1995) can be used to estimate the current development stage of vegetation in relation to the maximum LAI-values (forests = 6 ± 0.015, grassland = 2.64; given by the NASA Land Data Assimilation Systems; Rodell *et al.*, 2004). The vegetation height was calculated and compared with measurements (Nikon Laser 550 AS rangefinder) of 80 representative trees in differently developed forest stands in order to get an estimate for accuracy of the computed development stage from the LAI. The current development stage of vegetation allows the approximation of root fractions within distinguished soil layers (including root cohesion and water uptake potential), vegetation surcharge, interception capacity and evapotranspiration. The root fraction for different soil layer depths is computed with a model proposed by Gale and Grigal (1987). We set a maximum root cohesion value (c_r) to 15 [kN m^{-2}] for all adult stands (Bischetti *et al.*, 2005, 2009), since the stability model only accounts for root reinforcement by adding c_r to soil cohesion. The root reinforcement is adapted accordingly with the decrease in root fraction when the LAI-computation revealed a younger development stage (cf. Figure 2B). Surcharge was approximated according to the register provided by Wartluft (1978). The change in interception capacity can be calculated with a simplified variant of the Rutter-Gash-interception-model

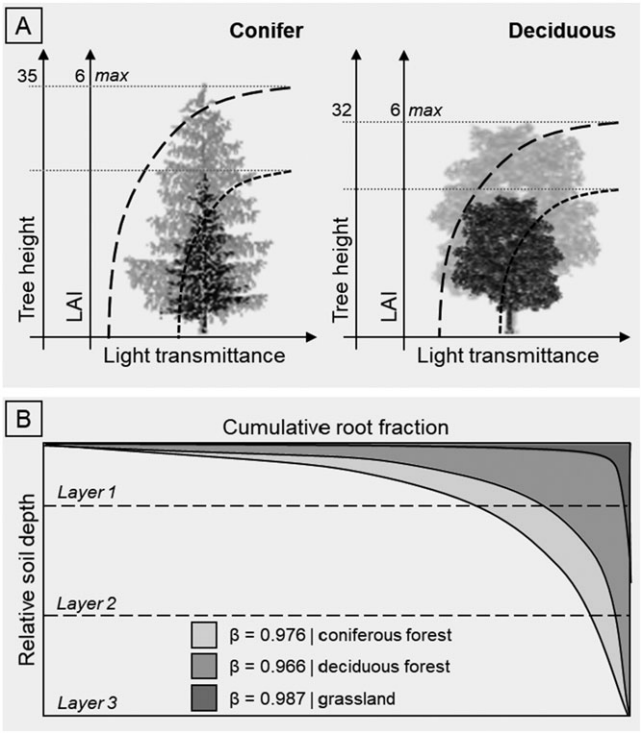

Figure 2. A: Concept of tree height estimation by light transmittance through a tree canopy. In the approach it is assumed that the amount of light halves by interception from the canopy with a rate of LAI = 1. When a maximum value of LAI is assigned to a maximum value of tree height, the apparent tree height can be estimated by the amount of transmitted light. B: Approximation of root fraction for different soil layers.

from Liu (1997). As adjustment for the computation with the Liu-model, we assumed that the whole amount of precipitation falls within one day at a single rainfall event. The reference evapotranspiration (ET_0) for the land cover scenarios 1 and 2 is calculated with the Penman-Monteith-equation (Zotarelli *et al.*, 2010; Penman, 1948; Monteith, 1965). ET_0 is additionally adapted by a crop coefficient of 0.85 (Verstraeten *et al.*, 2005) in scenario 2 (see chapter 'Slope stability modelling) in order to get an estimate of the potential evapotranspiration (ET_{pot}) in forested areas (Doorenbos and Pruitt, 1977; Hargreaves and Samani, 1985). For scenarios 3 and 4, we used an adapted the version of the Penman-Monteith equation that considers the stomatal conductance and resistance of leaves by the leaf-conductance-model of Stewart (1988). A summary of all processes, parameters or indices that are related to the vegetation cover and considered in the modelling procedure are listed in Table I.

Table I. Considered vegetation-related processes, parameters or indices with respective references distinguished for surface biomass, water assimilation and root biomass

Surface biomass and development	Reference
Normalised Differenced Vegetation Index (NDVI)	Rouse et al. (1973)
Leaf Area Index (LAI)	Sellers et al. (1996), Los et al. (2000), Rodell et al. (2004)
Light Transmittance (LT)	Bresinsky et al. (2008)
Surcharge	Wartluft (1978)
Interception capacity	Liu (1997)
Annual growth rate (y)	Houllier et al. (1995)
Reference Evapotranspiration (ET_0)	Zotarelli et al. (2010)
Potential Evapotranspiration (ET_{pot}) with crop coefficient	Verstraeten et al. (2005)
Potential Evapotranspiration (ET_{pot}) with leaf conductance	Stewart (1988)
Root fraction	Gale and Grigal (1987)
Root cohesion	Bischetti et al. (2005)

We linked the species-related phenological characteristics of forest stands with the annual temperature cycle and its seasonal impacts (e.g. development of a snow coverage) by implementing a Leaf Area Index Module (LAIM) that computes the development of LAI on a daily basis. The module is governed by environmental constraints and simulates the days of the vegetation period in daily time steps according to temperature and solar radiation. Leaf foliage and colouring of deciduous trees is stimulated after ten consecutive days above and five consecutive days below 5°C (cf. Konnert, 2004), whereas the periods for and leaf loss are set to 25 days. Leaf foliage within the same season after colouring is hindered by the day of the inflection point of solar radiation in the second half of the year. The performance of the LAIM was assessed for the hydrological calibration year 2016/17.

For the spatio-dynamic computation of land cover and vegetation parameters, we compiled the Land Cover Development Module (LCDM). The LCDM is linked to the LAIM and computes expansion, vertical growth and densification (in case of forests) of vegetated areas for each day within a vegetation period (n_i). With this, the development of the root fractions within different soil layers, surcharge, interception capacity and evapotranspiration can be calculated. Vertical growth of forest and densification are computed by the LCDM based on the growth functions that are used to approximate the development stage of vegetation.

Based on the information from the existing digital land cover maps, the potential increase of forested areas from within the vegetation period is computed and governed by the following constraints: i) forest growth emanates from existing forest edges; ii) the rate of spatial growth is limited to the spatial extent of forest area of the subsequent forest map; iii) expansion, densification and vertical growth of forest can only occur during the computed vegetation period by the LAIM; iv) the forest type, to which a new forest cell belongs depends on the forest type that is true for the next land cover map; v) a forest cell of the current land cover map is vanished when the cell is not declared as forest cell in the subsequent land cover map. An illustration of the procedure is illustrated in Figure 3.

The accuracy of the land cover expansion computed by the LCDM is compared with digital land cover maps from the years 1984, 1996, 2001 and 2006. Further technical details can be found in the Supporting Information.

Slope stability modelling

Derived vegetation parameters and connected processes, the annual development of LAI and the land cover dynamics computed by the LAIM and the LCDM were then coupled with the combined model STARWARS/PROBSTAB (Van Beek, 2002). It comprises the dynamic hydrological part STARWARS (*ST*orage *A*nd *R*edistribution of *W*ater on *A*gricultural and *R*e-vegetated *S*lopes) and the probabilistic geomechanical part PROBSTAB (*PROB*ability of *STAB*ility) and operates in a raster grid environment of the pcraster GIS (Karssenberg *et al.*, 2010). The soil column is represented by three different layers that function as hydrological reservoirs, considering infiltration of rainfall or snowmelt water into the topsoil layer, percolation from one layer to the subjacent layer, and lateral water flow from a higher to a lower adjacent raster cell. STARWARS computes dynamically the soil moisture contents and the groundwater

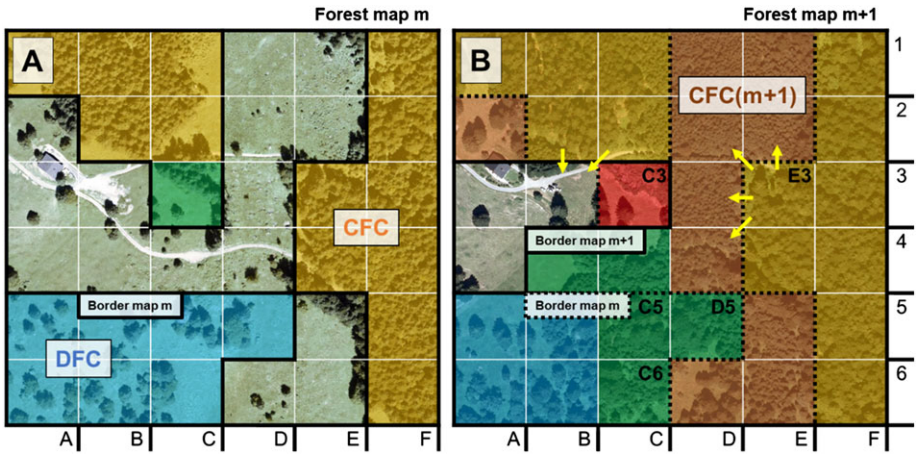

Figure 3. Visualisation of the functionality of LCDM in a raster environment. The assignment of the wood type class of a FC_{new} is defined by the subsequent forest map (m+1; red dashed line). Black arrows indicate the direction of possible forest expansion, emanating from the forest edge (black dashed line) of the current forest map m. [Colour figure can be viewed at wileyonlinelibrary.com]

level response to infiltrated water from a given precipitation input. The computed hydrological information of each layer (e.g. increase of pore water pressure and the subsequent loss of matric suction) is then forwarded to PROBSTAB that accounts for spatio-temporal changes in mechanical stability and calculates both factor of safety (FoS) and failure probability (P_f) for each raster cell. In this study, slope stability variations were modelled with a time interval of $\Delta t = 1$ day, since the majority of the input data comprise daily average values.

Four different soil type classes (STC), comprised by cambisols, colluvisols, initial soils and hydromorphic soils, were regionalised based on 58 sampling locations (18 soil profiles, 37 Pürckhauer samples, 3 corings). Soil horizons were distinguished and described at the 18 soil profile locations, from which dry bulk weight and textural composition of two to three samples per soil horizon (46 in total) were analysed in the laboratory. Geotechnical and hydraulic parameters were derived from pedotransfer functions (PTF) of Saxton and Rawls (2006). Organic matter of the topsoil layers was estimated in the field (cf. AG Boden, 2005). Soil thickness was approximated based on a model proposed by Catani *et al.* (2010) using derivatives of a 20 m × 20 m Digital Terrain Model (DTM), such as curvature, the position along the slope profile and slope gradient.

Hydrological monitoring is conducted on four locations along the slope. Piezometers for groundwater measures are installed at two downslope locations, whereas two stations at the upslope part are additionally equipped with devices for measuring soil moisture content in four depths (PR2/4), soil temperature and precipitation (tipping bucket rain gauge). Additional meteorological data including wind speed, solar radiation and air temperature was obtained from the National Survey for Meteorology and Geodynamics of Austria (ZAMG).

The model is applied for a total of four different land cover scenarios to compare the effect of different stages of land cover parameterisation (Figure 4):

- scenario 1: The land cover consists of sealed areas, bare soils and grassland. Forests are considered as grassland in order to simulate the effects of a low vegetation cover. Scenario 1 functions as 'reference' scenario for comparison with the others scenarios;
- scenario 2: Forests are treated as uniform (mixed and dense stands), with constant values for all vegetation parameters and evapotranspiration is calculated by means of crop factors;
- scenario 3: The calculation of LAI is used to estimate the development stages of vegetated areas and to derive vegetation parameters. The LAIM computes the annual LAI development;
- scenario 4: Similar to scenario 3, but LCDM is linked to the LAIM to account for forest expansion, vertical growth and densification effects.

A warming up of the model for 20 average years with average hydrological conditions, derived from the meteorological analyses, was performed to compute a hydrological balance and to estimate initial conditions. We calibrated STARWARS at the piezometer locations using the PEST-code (Model-Independent Parameter Estimation, Parameter Estimation Inc., 1999), based on the Marquardt–Levenberg least-squares algorithm for non-linear parameter optimisation (Marquardt, 1969). The first-order second-moment (FOSM) method (Ang and Tang, 1984) was used to compute P_f. The FOSM-method considers a normal distribution curve based on the standard deviation of geomechanical input parameter to account for their possible variation. By applying the FOSM-method it is possible to indicate the sensitivity of the model to distinct mechanical parameters and the model uncertainty towards the estimation of those parameters. We used the computed $P_{f,max}$-values to calculate the AUC for all performed scenarios to evaluate the predictive performance of the model based on the detected landslide scarp areas from the inventories of 1999 and 2005. Previous studies, however, revealed that the strongly generalizing AUC might react insensitive to the variation of input parameters in physically based slope stability models (de Lima Neves Seefelder *et al.*, 2017; Mergili *et al.*, 2017). Therefore, we calculated in addition a Factor of Conservativeness (FoC) as an indicator to assess the spatial conservativeness of the model output, ranging from 0 to infinity, where FoC = 1 depicts a perfectly conservative model result (cf. Mergili *et al.*, 2014). Values of FoC < 1 indicate a spatial underrepresentation of predicted unstable raster cells, whereas FoC > 1 an overestimation. Release raster cells (FoS < 1.0) were classified as either correctly or incorrectly predicted by the model.

Results

Environmental data and land cover dynamics

The comparison of the soil depth indicated an acceptable accuracy of the predicted soil depths (Figure 5A), resulting in

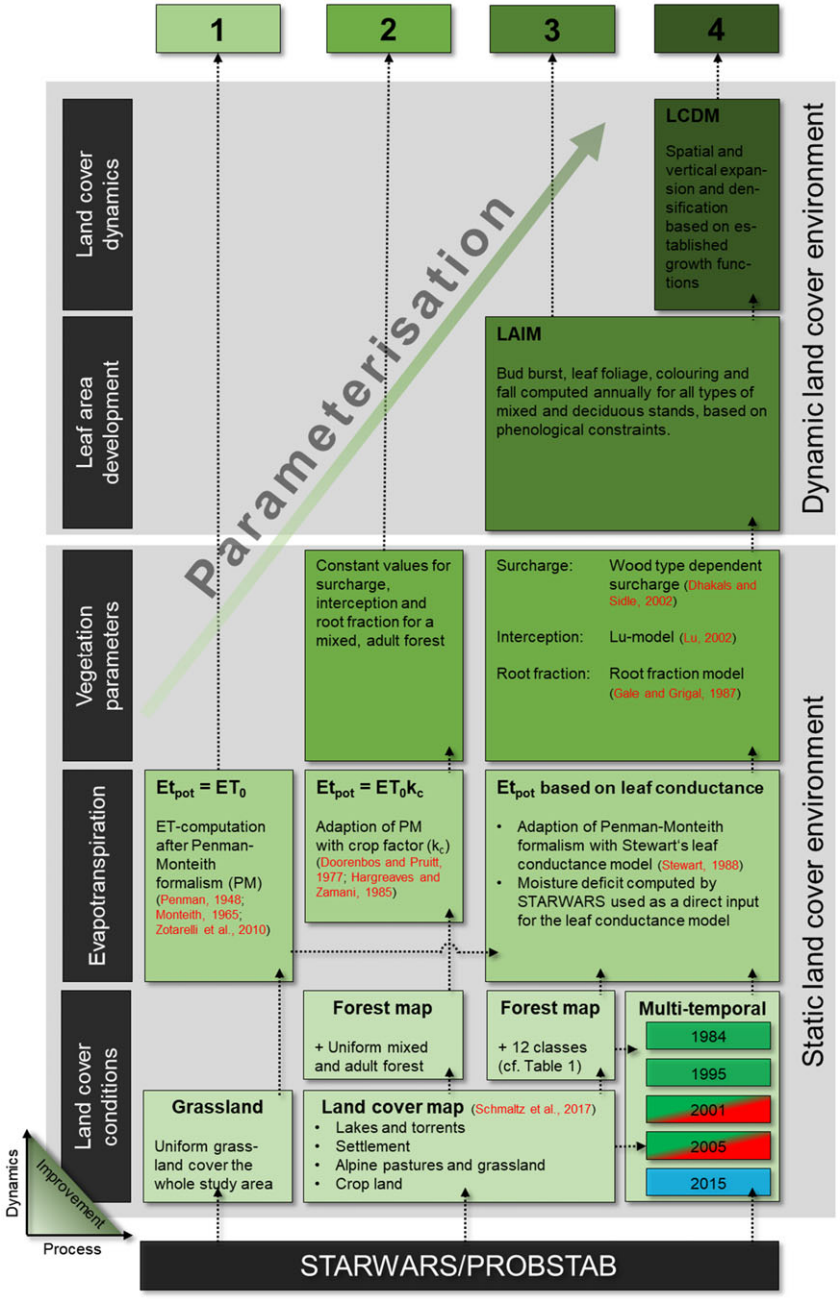

Figure 4. Strategy for land cover parameterisation of the four scenarios. Colours for the multi-temporal land cover maps indicate the use of the respective map in the modelling procedure: green = modelling and calibration; green/red = modelling and validation; blue = calibration of the hydrologically monitored years 2016/17. [Colour figure can be viewed at wileyonlinelibrary.com]

a linear relation to the predicted soil depth values with a coefficient of determination of $R^2 \approx 0.79$. The LAI-based light transmittance approach for vegetation height estimation yielded heights for grassland not more than max. 0.3-0.4 cm throughout the whole study area and the estimated forest stand heights are in acceptable accordance with ground-truth data ($R^2 \approx 0.85$, Figure 5B). Bare soil, streets or buildings were not classified as vegetated due to the low reflectance values.

The recorded soil moisture data by the PR2/4 indicate an immediate reaction of the topsoil (in ~15 cm depth) towards infiltration of rainfall/snowmelt and thus a fast wetting of the topsoil layers for both locations S1 and S2 (Figure 6). The soil moisture content reduces remarkably for both locations during winter period but much more at station S2, which might be interpreted by the sandy soil structure of the deep (and partly loose) morainic material that is apparent in this area. Measurements at station S2 indicate a beginning of the snowmelt season before the snow was fully gone (~day 410), which is similarly observable at station S1, but not that pronounced (cf. Fig. 6A1+2). Both snowmelt periods are similarly modelled by STARWARS as seen within the blue coloured areas in figure 6A. Both, the increase of the soil temperature and soil moisture content recorded by the sensors appear almost simultaneously, which strongly indicate the reduction of the snow cover in spring and indicate a good representation by STARWARS.

The module computed a vegetated period of ~212 days in 2016 and ~170 days for 1999 (Figure 7). Herein, a vegetation period is considered from the day of first bud burst or leaf foliage, respectively, to the day when the last leaf falls from the canopy. In this regard, it has to be highlighted that 2016 and 1999 depict exceeding warm (2016) and cold (1999) years with late warm periods or an extensively snow prone winter. The module represents reliably the observed phenological cycles of both mixed and deciduous trees for the calibration year. The particularly warm year of 2016 is reflected in the module results. Warm periods (e.g. mid to end of November) are

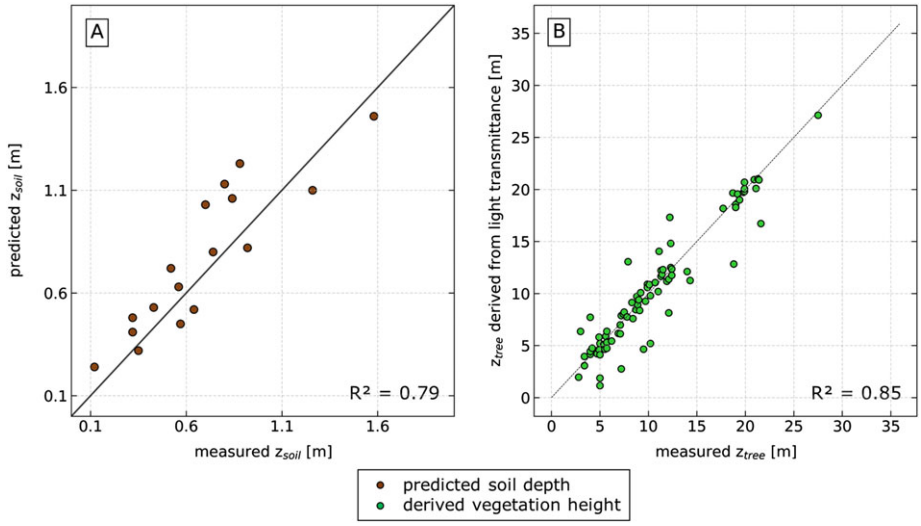

Figure 5. A: Predicted and measured soil depths (z_{soil}). B: Derived (predicted) and measured vegetation heights (z_{tree}). [Colour figure can be viewed at wileyonlinelibrary.com]

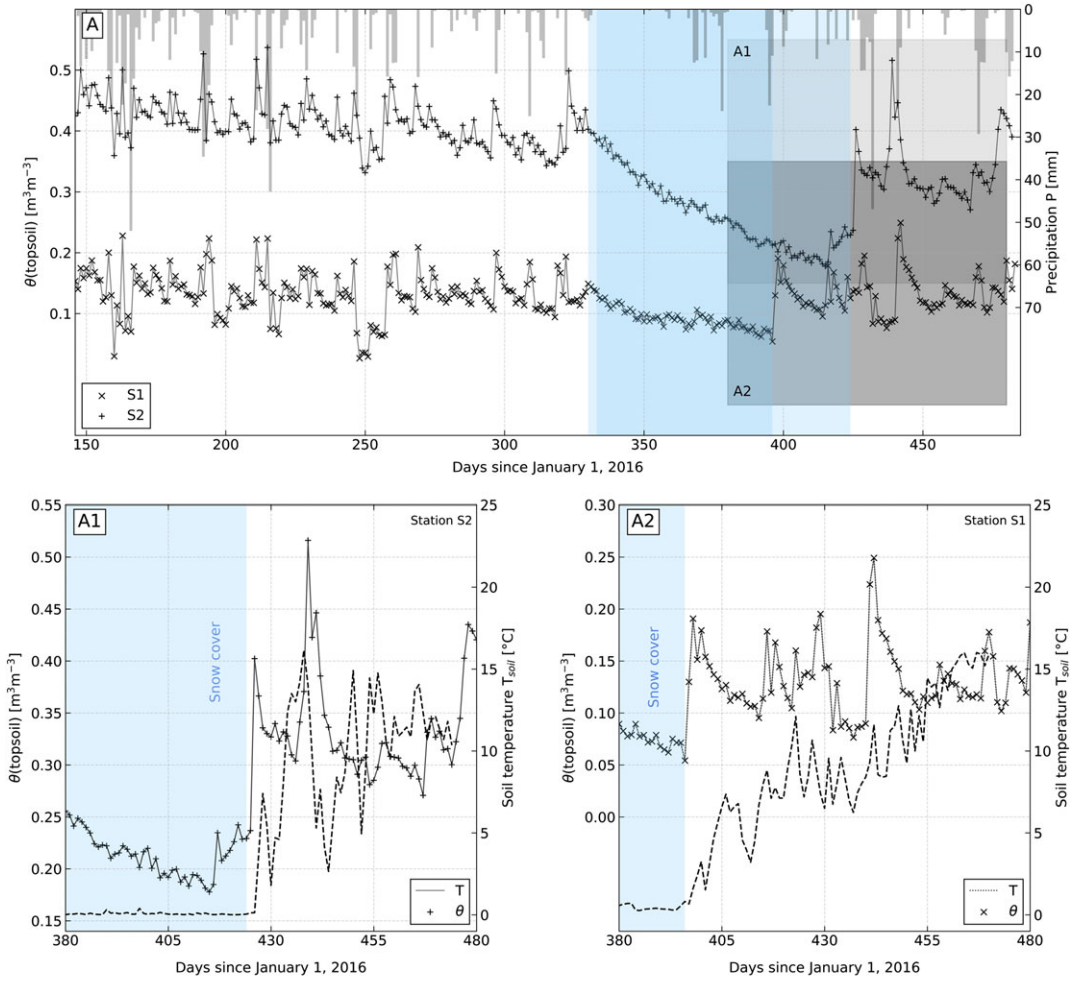

Figure 6. A: Measured soil moisture fluctuations at the stations S1 (blue) and S2 (green) with daily cumulated precipitation (grey bars). Blueish coloured areas indicate modelled snow cover at S1 (lighter blue) and S2 (darker blue). Details for A1 and A2 are given in the greyish frames. A1+A2: Details for soil moisture contents at the end of snow period (blueish) and at snowmelt. The red line shows the measured soil temperature at 15 cm depth. [Colour figure can be viewed at wileyonlinelibrary.com]

represented relatively well, particularly in the downslope parts. The snow melt season is observable for both years based on field observations and the available meteorological data. The inclusion of the inflection point of R_s as a constraint for leaf colouring initiation successfully hinders the module to compute potential bud burst in autumn, as it was the case in 2016, where a remarkable warm period is observable in November. Forests in higher located areas have a recognisable

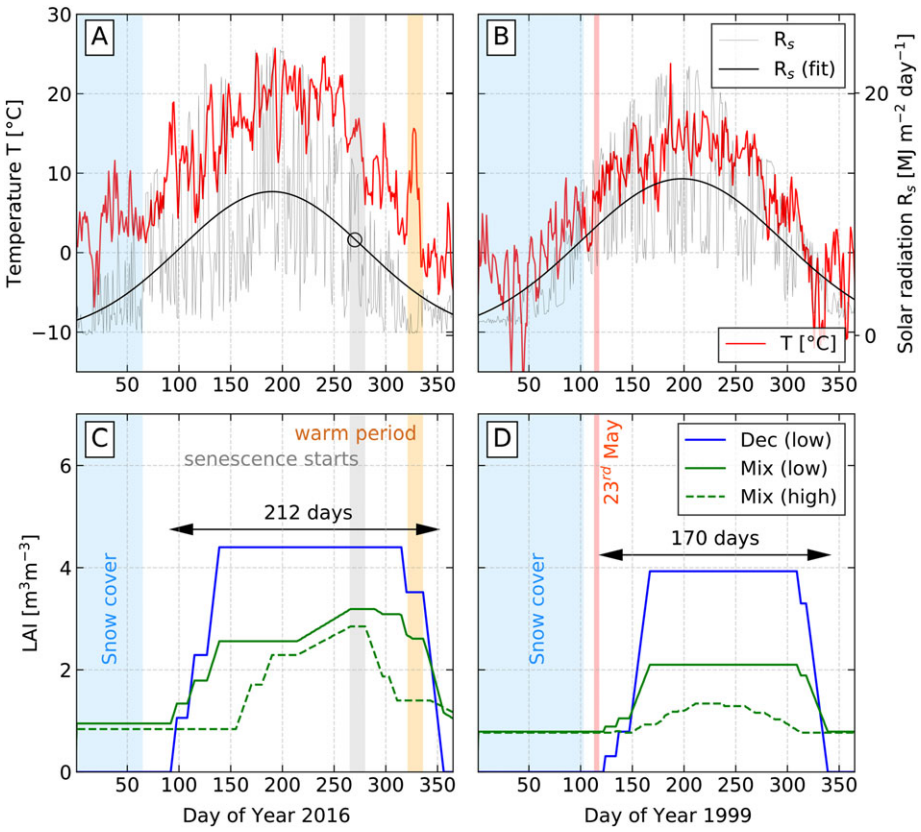

Figure 7. A: Temperature cycle of the calibration year 2016. The inflection point of the Gaussian fitting curve (black line), at which the growth season module considers leaf colouring (leaf senescence) due to the drop of solar radiation, is indicated with a circle. A warm period in autumn 2016 is indicated with an orange stripe. B: Temperature cycle of the validation year 1999 with indication of the triggering event (May 23, 1999) after the snow melt season (red stripe). C+D: Computed growing seasons for the years 2016 (calibration) and 1999 (validation). [Colour figure can be viewed at wileyonlinelibrary.com]

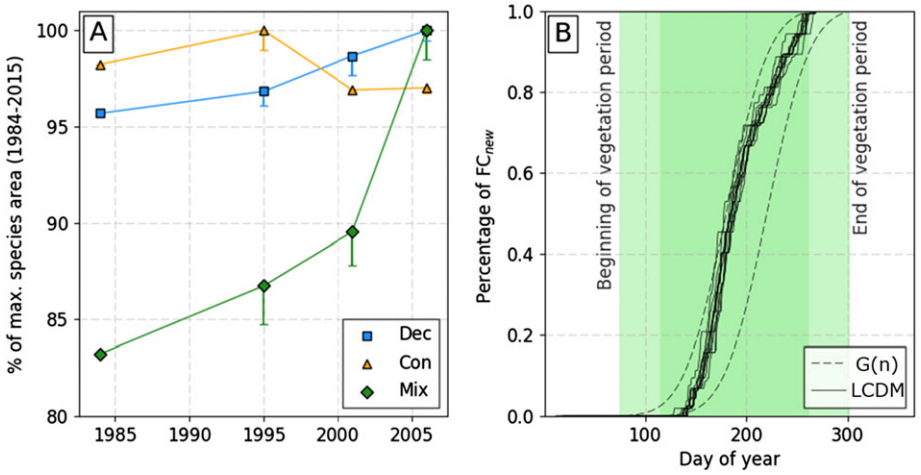

Figure 8. A: Percent of the maximum area per distinguished forest species or type, respectively, for the modelled period between 1984 to 2005. B: Percentage of predicted new forest cells (FC_{new}) during the computed vegetation periods for all modelled years and in comparison to the cumulative distribution function G(n). [Colour figure can be viewed at wileyonlinelibrary.com]

shorter vegetation period and less development of leaf area, which clearly reflects the response of vegetation phenology towards the apparent temperature gradient of the study area.

The LCDM-results over the years 1984 and 2005 show highest mismatch of the modelled areas for mixed forests in 1995: 2 %, 2001: 1.75 %, and 2005: 1.5 % compared to conifer or deciduous forests (Figure 8A). The mismatch is always negative because the module was not designed to predict expansion that exceeds the forested area of the subsequent land cover map. Mixed forest stands show the highest spatial increase between 1984 and 2005, particularly between 2001 and 2005. In contrast, conifer stands used as timber forests experienced a decrease between 1995 and 2005. Among all forest classes, 1995 yielded the highest percentage of mismatched areas compared to others (Dec: 0.75 %, Con: 1 %, Mix: 2.5 %). On an annual basis, the prediction of forest expansion is governed by the temperature-dependent growth cycle and a random effect. Thus, the annual expansion within the vegetation period can be described by a cumulative distribution function, similar to the one used for vertical growth in

this study. Figure 8B shows the performance of the expansion module for all modeled years by representing the percentage of new forest cells (FC_{new}) throughout the modelled year. As observable in Figure 8B, the percentage of predicted FC_{new} follows quite well the curve that is given by G(n) for both speed of expansion when the vegetation period starts and ends, as well as the date of the inflection point, which determines the maximum rate of expansion during the vegetation period.

Groundwater and slope stability

The drop of the measured groundwater table as detected by the divers is clearly observable for the winter 2016/17 at all piezometer locations (Figure 9). At station S2, this drop is rather not incisive, whereas the reaction on precipitation events is partly stronger compared to the other stations. The results of the modelled land cover scenarios show that STARWARS reacted sensitively to the absence of data related to high vegetation cover (scenario 1). In comparison to the other scenarios, the absence of a remarkable forest cover is not able to repress the modelled groundwater table in a way that it fits with the observed groundwater levels from the divers. The representation of a fully mature mixed forest without any differentiations in the stand structure (scenario 2) is also not capable to represent the observed groundwater fluxes reliably. Except for the location of piezometer P2, scenario 4 shows the lowest RMSE among all scenarios, whose average RMSE equals 4.2 cm. However, scenarios 3 and 4 show quite similar patterns in the prediction of groundwater fluxes after calibration.

Table II. AUC and FoC results for all applied scenarios and the triggering events from 1999 and 2005

	Scenarios (AUC| FoC)			
Event	Scenario 1	Scenario 2	Scenario 3	Scenario 4
1999	0.56| 720	0.65| 0.05	0.71| 0.61	0.76| 0.71
2005	0.55| 831	0.63| 0.10	0.70| 0.63	0.74| 0.71

PROBSTAB over-estimates unstable areas for scenario 1 (no forest, only grassland vegetation) with around 22-26 % of unstable raster cells (FoS < 1) over the whole area for the triggering events of 1999 and 2005. This explains unreliably high values of the FoC (720-831) since landslide release areas are predicted well, whereas stable areas are considerably underrepresented at the time of failure. In contrast, the assumption of a fully mature, dense and mixed forest for all forested areas (scenario 2) leads to a under-estimation of unstable raster cells with a spatial inaccuracy (FoC = 0.05-0.1; cf. Table II).

Instability only occurs in topographically landslide-prone areas such as very steep slopes that are undercut by torrents but still experience a large amount of surcharge from vegetation. Scenarios 3 and 4 yield the best spatial predictions of slope instability. Figure 10 shows FoS-values for the triggering event of 1999 (A and B) and 2005 (C and D) with the most prominent slope failures for the respective triggering event (1999: 1-4; 2005: 5-6). FoS is considerably lower for scenario 4 in forested areas (av. FoS ~ 0.9) compared to scenario 3. Failure cells that were computed by scenario 4 are spatially more accurate than those of scenario 3 for the prominent landslides in 1999 and 2005. In fact, FoC-values of both triggering

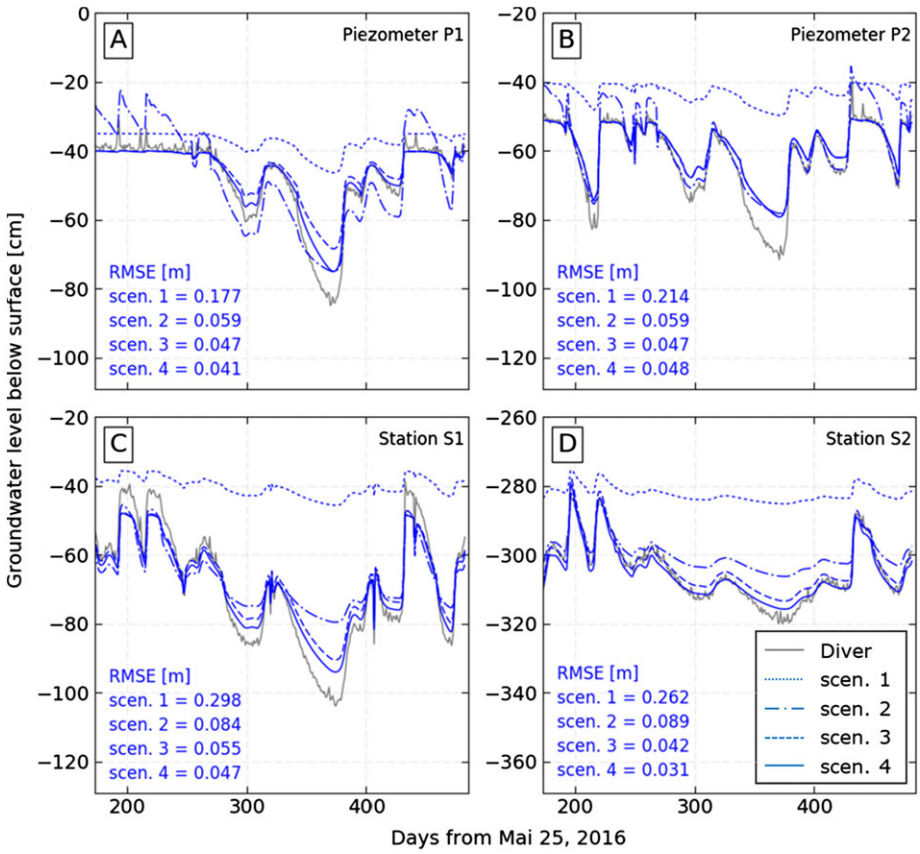

Figure 9. Measured groundwater table by the divers (grey) at all four locations. Results of the predicted groundwater fluctuations after calibration of all four scenarios are indicated with blue lines. RMSEs are given for all locations and scenarios (abbreviated as 'scen.'). Note y-axis values are set to similar intervals to ensure comparability between the four locations and increase readability of the plot, but value ranges differ due to different piezometer depths. [Colour figure can be viewed at wileyonlinelibrary.com]

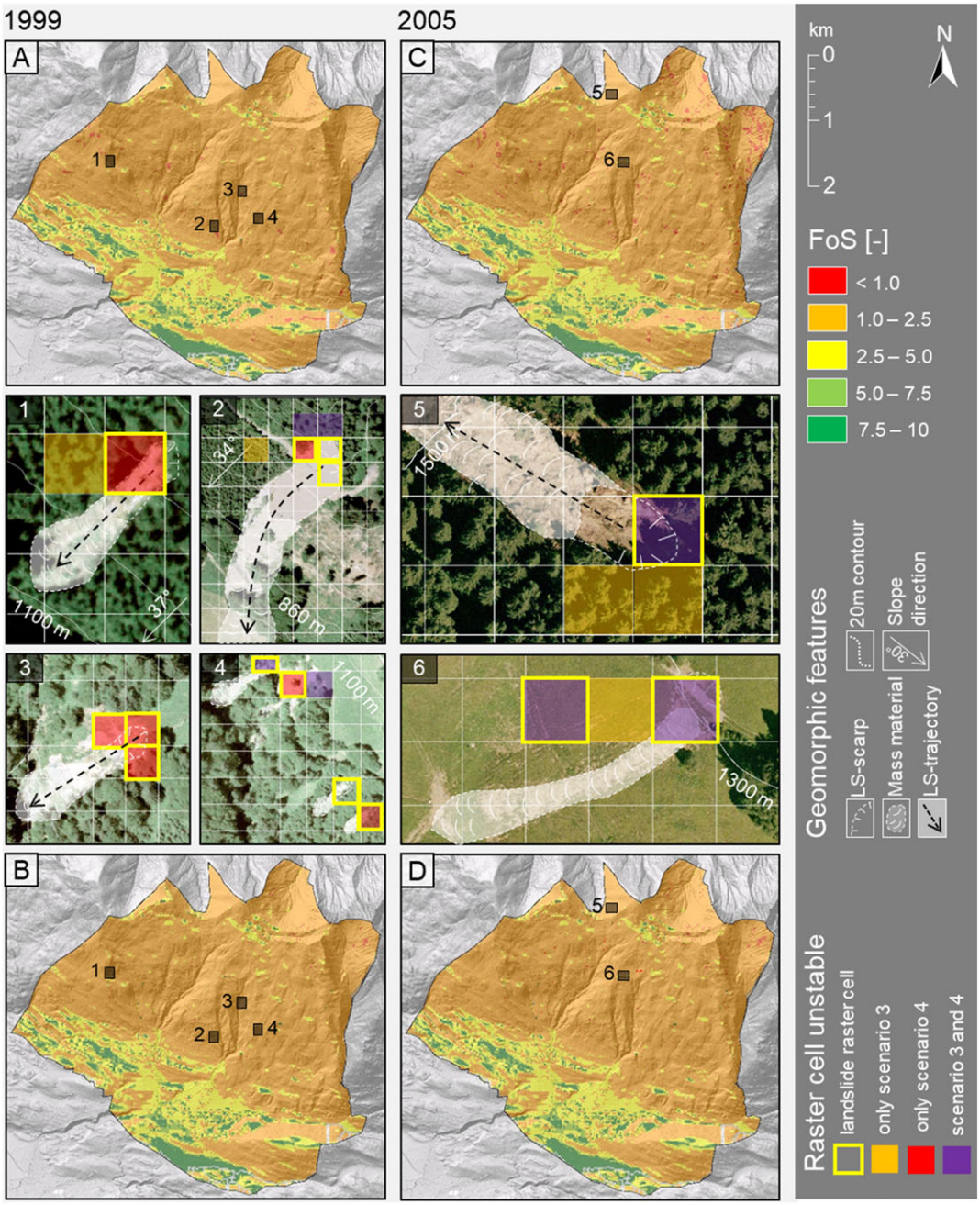

Figure 10. Factor of Safety of the modelled triggering events from 1999 and 2005 for scenario 3 (A and C) and scenario 4 (B and D). Details of prominent landslides (including geomorphic features) and the spatial accuracy of the predicted failure cells are indicated in pictures 1-6. [Colour figure can be viewed at wileyonlinelibrary.com]

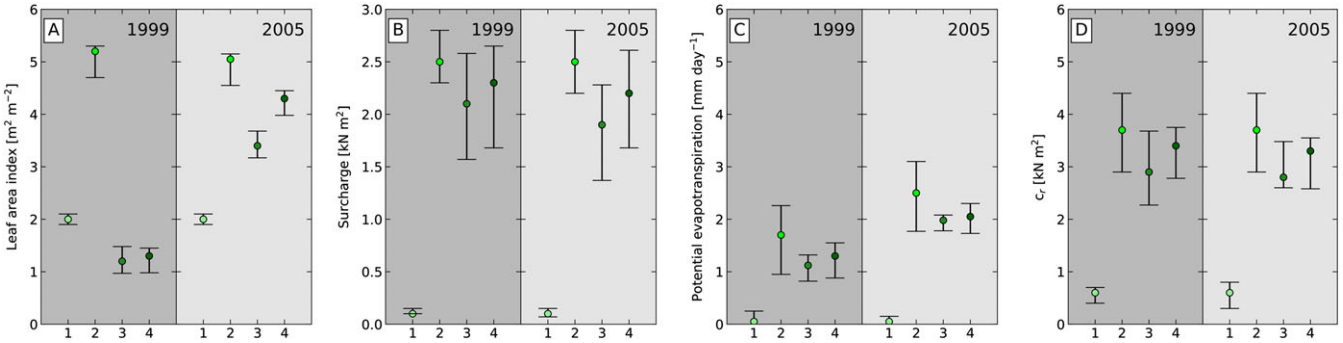

Figure 11. Parameter values ranges of LAI (A), surcharge (B), E_{pot} (C) and c_r (D) modelled by all scenarios (1-4) for both triggering events (1999, 2005). [Colour figure can be viewed at wileyonlinelibrary.com]

events for scenario 3 are relatively similar to those of scenario 4 (0.61-0.63 and both 0.71), indicating a conservative prediction of failure cells for both scenarios (cf. Table II).

Scenario 1 shows low parameter ranges for LAI, surcharge, ET_{pot} and c_r compared to the values modelled by the other scenarios (Figure 11). In contrast, scenario 2 yields always the highest values for all parameters and both triggering events. Albeit the fact that the modelled parameter ranges for scenarios 3 and 4 appear to be quite similar, interesting differences are observable. Both scenarios show low average LAI-values (1.1 and 1.3) at the detected landslide scar areas for the triggering event in May 1999 (Figure 11A), whereas leaf area development is not considered in scenario 2 and thus LAI-values remain high. ET_{pot}-values are low for all scenarios (but highest for scenario 2). However, higher differences can be observed between scenarios 3 and 4 for surcharge (2.0 and 2.3 kN m^{-2}) and c_r (2.9 and 3.4 kN m^{-2}). This reflects the consideration of land cover development in scenario 4 (which is not considered in scenario 3), since surcharge and cr are the parameters that are mostly affected (besides forest expansion) by vegetation growth modelling in the LCDM.

The predictive performances of all scenarios for the modelled triggering events are presented as ROC-curves and AUC-values in Figure 12. In general, no distinct difference in performance is recognisable between the modelled events (1999 vs. 2005). However, it is clearly observable that the models performed substantially different in response to varying land cover scenarios. Scenario 1 predicts unstable areas well but under-estimates stable areas, which is observable in the ROC-curves for both events and low AUC values (0.55 and 0.56, indicating an almost random model). Performance results of scenario 2 indicate a better prediction for unstable areas compared to scenario 1. Scenario 3 and 4 perform relatively similar (AUC-values of ~0.71 and 0.75), indicating an acceptable predictive performance of both unstable raster cells and stable areas.

Discussion

Performance of the land cover modules

The estimation of vegetation heights by the LAI-based light transmittance provided reliable results for both grassland and forests. Considering a recording date of the nir-false-colour image in summer, the estimated heights of grassland and alpine pastures with not more than 40 cm depicts a quite good estimate for grass height in this period, especially for rough pastures that are mown twice per year or grassland areas that are typically used for grazing. Even though the estimation results for forest stand heights seems in good agreement with ground-truth data (RMSE $<$ 2 m), the results have to be interpreted with caution. Both the light transmittance approach as well as the measurement of representable trees within a stand by a laser device may contain a variety of error sources. The approach chosen in this study considers the transmission of photons with a zenith angle of 0 degrees. However, Canham *et al.* (1994) have shown that light transmittance might decrease with a higher zenith angle. Thus, light transmittance through the canopies should be corrected according to the recording angle of the airborne-based orthophoto, which might result in a more reliable estimation. Regardless of the chosen zenith angle, light transmittance is strongly dependent on the leaf shapes and the canopy structure of the trees and stands (cf. Montgomery and Chazdon, 2001) – both species- or stand-reliant parameters. Since the raster resolution selected for all analyses in this study entails a generalisation of all physical parameters, the importance of leaf shapes and canopy structure for light transmittance estimation can be considered negligible. A raster with 20 m × 20 m raster cell size depicted an acceptable compromise for our purposes, since multiple previous studies highlighted rather worse modelling results with high raster resolutions (Tarolli and Tarboton, 2006; Keijsers *et al.*, 2011; Cislaghi *et al.*, 2017). However, we stress that for higher resolved rasters, species-reliant parameters and the angle of the recorded orthophoto can have an impact on the result. Moreover, we assumed a maximum LAI of 6 (as suggested in Rodell *et al.*, 2004), which indeed can differ remarkably from the true maximum LAI in the study area. In this regard, the use of airborne and/or terrestrial LiDAR-based remote sensing data could increase the accuracy of considered values for (maximum) LAI and apparent vegetation heights.

The LAIM reliably represents both shifting/shortening of the vegetation period depending on the annual temperature cycle (cp. 2016 and 1999 in Figure 7C+D). It has to be highlighted that the module considers a certain "speed of leaf fall", which might slow down the loss of leaves in warm autumns and leads to a decreasing value of LAI even in the late autumn. However, this does not necessarily lead to an unnaturally higher rate of transpiration or water assimilation, since the plants are not

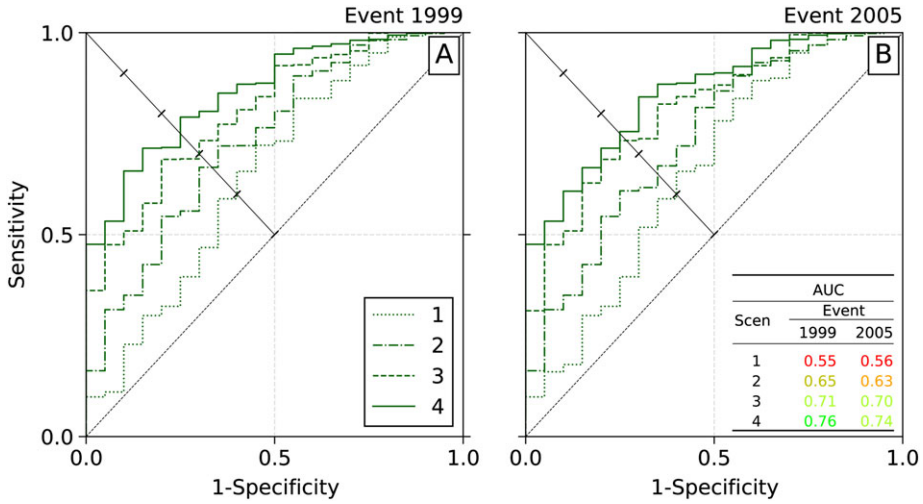

Figure 12. ROC-curves of all modelled land cover scenarios (line types) for the event of 1999 (A) and 2005 (B) based on the respective event-based landslide inventories and the computed P_f-values. The AUC values of all scenarios are given in B. [Colour figure can be viewed at wileyonlinelibrary.com]

stimulated for considerable amounts of transpiration (and thus water uptake) when the temperature is low (Aroca *et al.*, 2011). Hence, the remaining LAI in late autumn has no hydrological effects on the slope stability for the Dreiklang region. In general, the course of LAI throughout the year is in accordance to the suggested phenological cycles for leaf development in Rodell *et al.* (2004). The implementation of the inflection point of the R_s-cycle depicts a robust estimate for limiting re-foliage of leaves during late warm periods. However, a detailed representation of autumn phenology is reliant on more physical properties (Chmielewski and Rötzer, 2001) and thus requires more phenological information that were not available for this study. Interestingly, the LAIM computed leaf foliage and bud burst for the year 1999 only shortly before the landslide-triggering event at May 22. Considering a good prediction on the LAIM for bud burst for the year 2016 (± 3-5 days) it can be assumed that no reliable leaf coverage was apparent during the rainfall event that caused the landslides in 1999. A substantial leaf cover (such as LAI<1 for deciduous stands observed for the landslide locations in 2016 at the same day) could have intercepted considerably higher amounts of rainfall than it was possible in 1999. Since the amount of rainfall, however, was extreme (251 mm day^{-1}) on the supposable triggering date, the potentially infiltrated rainfall might have exceeded the infiltration capacity. Hence, it remains questionable whether the higher leaf coverage in 2016 would have prevented slope instabilities at an extreme rainfall event like in 1999.

The results indicate that the LCDM is able to compute spatial forest expansion annually and over long periods reliably with a relatively small percentage of under-representation for all apparent forest classes (Figure 8). However, several limitations of the applied LCDM have to be mentioned: 1) albeit the module relies on empirical parameters, the expansion of land cover is strongly dependent on a random effect. We intended to cope with the fact that forest expansion relies not only on meteorological parameters or phenological properties (Chmielewski and Rötzer, 2001) but on species-related peculiarities that are difficult to determine for modelling approaches at stand-scale. Thus, introducing this random effect in the module helps to define speed and direction of forest expansion but consequently leads to a meaningful uncertainty in the subsequent prediction of slope stability. 2) Since the prediction of forest expansion in the module relies on the abovementioned random effect, the use of a subsequent forest map, which defines types and densities (dense or sparse) of forest stands, is necessary to correct and validate the modelling results. 3) Decay is not considered in the module and the representation of harvested areas is dependent on multiple forest maps (as mentioned in the previous point). However, for model runs over multiple decades, processes that promote decay should be considered in comparable modules.

Impact of parameterisation and model complexity

According to the results of the hydrological calibration of STARWARS, the consideration of a sophistically parameterised land cover (scenarios 3 and 4) yields the best representation of groundwater fluctuations compared with the data recorded by the divers (average RMSE less than 5 cm). However, several patterns among the applied scenarios are recognisable and motivate different interpretation. STARWARS enabled considerably better calibration results for scenario 3 and 4 (compared to scenario 2) at stations S1 and S2, which are located in adjacent areas of the timber line (cf. Figure 9). At lower locations (P1 and P2) the differences between scenario 2, 3 and 4 are less significant. This strongly indicates that forests that are located upslope of the monitoring stations might have a stronger impact on the groundwater balance than at locations where forests are farer away. The calibration results for scenario 1 throughout all locations indicate a incapability of the model to estimate groundwater tables reliably. This supports the statements of Meng *et al.* (2014) and modelling observations of Malet *et al.* (2005) that a landscape with a substantial forest coverage is able to repress groundwater tables remarkably (cf. Sidle and Ochiai, 2006, Sidle and Bogaard, 2016, Cohen and Schwarz, 2017), which is not represented in scenario 1. Indeed, the consistent over-estimation of groundwater level leads to either permanently unstable areas, which are in fact stable under most conditions, or to instability for unrealistic triggering events with little amount of rainfall. The repression of groundwater by vegetation is largely better represented by scenario 3 and 4, which omits unrealistic stability conditions when no triggering event is simulated.

However, the modelled groundwater tables cannot explain the better predictive performance of scenario 4 compared to scenario 3. Since both scenarios predict slope failures similarly well, a better performance of scenario 4 can be explained by a better stability prediction in areas, where no landslide scarp was detected but modelled as unstable in scenario 3. A reason for this might be that the LCDM applied in scenario 4 computes land cover development, which has a strong impact on the increase of either root cohesion itself due to the growth of forest stands. Thus, root reinforcement is more developed at time of failure in scenario 4, which leads to a more accurate prediction of stable areas that would have been modelled as unstable in scenario 3.

In this regard, it can be stated that the prediction of unstable areas with an acceptable predictive performance and conservative spatial accuracy demands greater efforts in the representation of land cover in case of the Dreiklang region. Similar findings were highlighted in Band *et al.* (2012) for particularly small shallow landslides within forests. Indeed, more effort in the parameterisation of land cover properties in the model pays of and both stable and unstable areas can be predicted in a more reliable way (cf. Band *et al.*, 2012, Hwang *et al.*, 2015), which we can support in our study. It has to be stressed that (at least for the Dreiklang area) the obtained predictive performance was not substantially higher with a more complex parameterisation (e.g. performed in scenario 4). However, a closer look at the respective maps provided evidence of spatially more accurate predictions. Particularly the implementation of the LAIM (scenario 3) increased the reliability of the model compared to a uniform forest (scenario 2). This indicates that the hydrological balance of a hillslope landscape is simulated better when land cover is more reliably represented, e.g. by seasonal changes water uptake potential driven by the amount of leaves and thus soil moisture conditions. This increases the prediction of hydrologically triggered slope instabilites or the simulation of the multi-annual variation of slope stability. However, the results also reveal that rather geomechanical properties, as the leading one additional root reinforcement that is deployed to the failure plain, are more important to predict unstable areas at the time of failure.

Further comparable studies, however, should evaluate first if the labour costs of implementing code-modifications that enable a representation of spatially distributed land cover dynamics (as performed with the LCDM in this study) can outballance the benefits of a slightly better prediction of slope instabilities. Based on the simulation results, we can accept our hypothesis that an increase of model complexity and land cover parameterisation enhances the predictive performance (from AUC of 0.65 to 0.71 and 0.76, respectively) and the spatial conservativeness of predicted unstable areas (0.63 and 0.71

with LAIM and LAIM+LCDM compared to 0.05 and 832 for a uniform grassland cover or a uniform and static forest cover).

Conclusion and outlook

We compared simulations with four different levels of land cover paramaterisation adopting the dynamic slope stability STARWARS/PROBSTAB. Therefore, we compiled two dynamic land cover modules, considering annual leaf area development (LAIM) as well as land cover expansion, densification and vertical growth of forest (LCDM). The implementation of the LAIM into the slope stability model (scenario 3) improved the predictive performance (AUC=0.71) and spatial conservativeness of the predictions (FoC=0.63), compared to scenario 1 (AUC=0.55, FoC=832) for a uniform grassland cover, or scenario 2 (AUC=0.65, FoC=0.05), where a uniform and stable forest without leaf area development is considered. The LCDM in combination with the LAIM (scenario 4) performed best (AUC=0.76, FoC=0.71). The following points can be summarised based on the findings from our land cover and slope stability simulations:

i) The absence of forest in a modelling procedure cannot reflect accurate stability conditions of a landscape.
ii) Simple parameter estimates for vegetated areas (in particular forests) in a dynamic slope stability model might lead to an over-estimation of the stabilising potential that is provided by the vegetation cover.
iii) The consideration of land cover development stages and seasonal variations of leaf area improves the dynamic reproduction of slope hydrology and the prediction of slope stability variations.
iv) Dynamic modelling of land cover in combination with leaf area variations increase the accuracy of predicted unstable areas due to a better approximation of root reinforcement at the time of slope failure.

Furthermore, it can be hypothised that the application of the LAIM and the LCDM (or comparable applications) might have a greater effect on the explanatory power of the model when landscapes with more extensive forest cover changes are investigated. However, despite the greater effort of land cover parameterisation, most of the land covers distinguished in this study rely on generalisations and compromises, particularly in forested areas since ground truth data are absent and hard to compile for larger regions. Several approaches are available that ensure a spatially extensive observation and compilation of vegetation data, such as airborne or terrestrial LiDAR-systems. Furthermore, new techniques allow to calculate allometric properties of single trees within forest stands relative precisely from LiDAR-point clouds. The implementation of those highly resolved allometric properties in the parameterisation of land cover (and forested areas in particular) could further enhance the sophistication of vegetation input parameters. Consequently, a more comprehensive and reliable land cover parameterisation can be performed with detailed allometric information, resulting in a conversion from approximated to actual measured vegetation input parameters. In fact, LiDAR-derived biomass data can improve the representation of vegetation in physically based slope stability models. Based on these findings, we expect a better and more reliable performance when vegetation parameters are not derived by optical remote sensing data sets, as performed in this study, but on the basis of more sophisticated LiDAR-data. Hence, we hypothesise that the inclusion of allometric land cover information from LiDAR measurements further enhances the computation of vegetation related processes and thus increase the prediction of potentially unstable areas in physically based slope stability models. However, our study shows that the better representation of leaf development and land cover dynamics leads to more accurate multi-annual simulation of the hydrological balance of a landscape and improves the prediction and spatial representation of slope failures.

Acknowledgements—The authors like to thank the Austrian Academy of Sciences. Furthermore, the authors thank Jakob Heinzle, Matthias Konzett and Christian Prochaska for supporting field surveys and the acquisition of data.

References

Ad-Hoc-Arbeitsgruppe Boden der Staatlichen Geologischen Dienste und der Bundesanstalt für Geowissenschaften und Rohstoffe (AG Boden). 2005. Bodenkundliche Kartieranleitung KA 5; mit 103 Tabellen und 31 Listen. Schweizerbart.

Ang AHS, Tang WH. 1984. *Probability concepts in engineering planning and design*. John Wiley & Sons Inc.: New York.

Arnone E, Caracciolo D, Noto LV, Preti F, Bras RL. 2016. Modeling the hydrological and mechanical effect of roots on shallow landslides. *Water Resources Research* **52**(11): 8590–8612.

Aroca R, Porcel R, Ruiz-Lozano JM. 2011. Regulation of root water uptake under abiotic stress conditions. *Journal of Experimental Botany* **63**(1): 43–57.

Band LE, Hwang T, Hales TC, Vose J, Ford C. 2012. Ecosystem processes at the watershed scale: Mapping and modeling ecohydrological controls of landslides. *Geomorphology* **137**(1): 159–167.

Baum RL, Savage WZ, Godt JW. 2002. *TRIGRS – A Fortran Program for Transient Rainfall Infiltration and Grid Based Regional Slope Stability Analysis, Open file report 02-424*. US Department of the Interior and US Geological Survey: Denver, CO.

Bellugi D, Milledge DG, Dietrich WE, Perron JT, McKean J. 2015. Predicting shallow landslide size and location across a natural landscape: Application of a spectral clustering search algorithm. *Journal of Geophysical Research: Earth Surface* **120**(12): 2552–2585.

Bischetti GB, Chiaradia EA, Epis T, Morlotti E. 2009. Root cohesion of forest species in the Italian Alps. *Plant and Soil* **324**(1-2): 71–89.

Bischetti GB, Chiaradia EA, Simonato T, Speziali B, Vitali B, Vullo P, Zocco A. 2005. Root Strength and Root Area Ratio of Forest Species in Lombardy (Northern Italy). *Plant and Soil* **278**(1-2): 11–22.

Bresinsky A, Körner C, Kadereit JW, Neuhaus G, Sonnewald U. 2008. Strasburger. *Lehrbuch der Botanik* **35**.

Burroughs ER, Thomas BR. 1977. Declining root strength in Douglas-fir after felling as a factor in slope stability. USDA Forest Service Research Paper INT-190: 27 p.

Burroughs ER. 1985. Landslide hazard rating for the Oregon Coast Range. Watershed management in the eighties. In *Proceedings of the Symposium on Effects of Forest Land Use on Erosion and Slope Stability (May 7-11, 1984)*. University of Hawaii, Honolulu: Hawaii USA; 265–274.

Canham CD, Finzi AC, Pacala SW, Burbank DH. 1994. Causes and consequences of resource heterogeneity in forests: interspecific variation in light transmission by canopy trees. *Canadian Journal of Forest Research* **24**(2): 337–349.

Catani F, Segoni S, Falorni G. 2010. An empirical geomorphology-based approach to the spatial prediction of soil thickness at catchment scale. *Water Resources Research* **46**: W05508.

Chirico GB, Borga M, Tarolli P, Rigon R, Preti F. 2013. Role of vegetation on slope stability under transient unsaturated conditions. *Procedia Environmental Sciences* **19**: 932–941.

Chmielewski FM, Rötzer T. 2001. Response of tree phenology to climate change across Europe. *Agricultural and Forest Meteorology* **108**(2): 101–112.

Cislaghi A, Rigon E, Lenzi MA, Bischetti GB. 2018. A probabilistic multidimensional approach to quantify large wood recruitment from hillslopes in mountainous-forested catchments. *Geomorphology* **306**: 108–127.

Cislaghi A, Chiaradia E, Bischetti GB. 2017. Including root reinforcement variability in a probabilistic 3D stability model. *Earth Surface Processes and Landforms* **42**(12): 1789–1806.

Cohen D, Schwarz M. 2017. Tree-roots control of shallow landslides. *Earth Surface Dynamics* **5**: 451–477 https://doi.org/10.5194/esurf-2017-10.

Crozier M. 1986. *Landslides: Causes, Consequences and Environment*. Croom Helm: London.

Crozier MJ, Glade T. 1999. Frequency and magnitude of landsliding: fundamental research issues. *Zeitschrift für Geomorphologie* **115**: 141–155.

Crozier MJ. 2010. Landslide geomorphology: An argument for recognition, with examples from New Zealand. *Geomorphology* **120**(1–2): 3–15 https://doi.org/10.1016/j.geomorph.2009.09.010.

Cruden DM, Varnes DJ. 1996. Landslides: investigation and mitigation. Chapter 3 – Landslide types and processes. Transportation research board special report 247. **5**: 451–477.

de Lima Neves Seefelder C, Koide S, Mergili M. 2017. Does parameterization influence the performance of slope stability model results? A case study in Rio de Janeiro, Brazil. *Landslides* **14**(4): 1389–1401 https://doi.org/10.1007/s10346-016-0783-6.

Dikau R, Brunsden D, Schrott L, Ibsen M-L. 1996. *Landslide Recognition: Identification, movement and causes*. John Wiley and Sons Ltd: Chichester.

Doorenbos J, Pruitt WO. 1977. *Crop water requirements*. FAO: Rome.

Endo T, Tsuruta T. 1969 The effect of the tree's roots upon the shear strength of soil. 1968 Annual Report, Hokkaido Branch, Forest Experiment Station: 167-182. English translation by Arata JM and Ziemer RR, U.S.Dep.Agric.For. Serv., Arcata, CA, USA.

Ewen J, Parkin G, O'Connell PE. 2000. SHETRAN: distributed river basin flow and transport modeling system. *Journal of Hydrologic Engineering* **5**(3): 250–258.

Friebe JG. 2004. Zur Geologie Vorarlbergs - eine Einführung unter besonderer Berücksichtigung verkarstungsfähiger Gesteine. *Vorarlberger Naturschau* **15**: 19–40.

Gale MR, Grigal DF. 1987. Vertical root distributions of northern tree species in relation to successional status. *Canadian Journal of Forest Research* **17**(8): 829–834.

Ghestem M, Sidle RC, Stokes A. 2011. The influence of plant root systems on subsurface flow: implications for slope stability. *BioScience* **61**(11): 869–879.

Glade T, Crozier MJ. 2005. The nature of landslide hazard and impact. In *Landslide hazard and risk*, Glade T, Anderson MG, Crozier MJ (eds). Wiley: Chichester.

Glade T. 2003. Landslide occurrence as a response to land use change: a review of evidence from New Zealand. *Catena* **51**: 297–314.

Gray DH, Megahan WF. 1981. Forest vegetation removal and slope stability in the Idaho batholith. USDA Forest Service Research Paper INT (USA). No. 271.

Gray DH, Sortir RB. 1996. *Biotechnical and Soil Bioengineering Slope Stabilization: A Practical Guide for Erosion Control*. John Wiley and Sons: EUA.

Greenway DR. 1987. Vegetation and slope stability. In *Slope Stability*, Anderson MG, Richards KS (eds). John Wiley and Sons: Chichester; 187–230.

Guzzetti F, Carrara A, Cardinali M, Reichenbach P. 1999. Landslide hazard evaluation: a review of current techniques and their application in a multi-scale study, Central Italy. *Geomorphology* **31**(1): 181–216.

Hales TC, Ford CR, Hwang T, Vose JM, Band LE. 2009. Topographic and ecologic controls on root reinforcement. *Journal of Geophysical Research: Earth Surface*, **114**(F3), F03013: 1-17.

Hales TC, Miniat CF. 2017. Soil moisture causes dynamic adjustments to root reinforcement that reduce slope stability. *Earth Surface Processes and Landforms* **42**(5): 803–813.

Hargreaves GH, Samani ZA. 1985. Reference crop evapotranspiration from temperature. *Applied Engineering in Agriculture* **1**(2): 96–99.

Heissel W, Oberhauser R, Schmidegg O. 1967. *Geologische Karte des Walgaues, 1:25.000*. Geol. B. A.: Vienna.

Houllier F, Leban JM, Colin F. 1995. Linking growth modelling to timber quality assessment for Norway spruce. *Forest Ecology and Management* **74**(1-3): 91–102.

Hwang T, Band LE, Hales TC, Miniat CF, Vose JM, Bolstad PV, Miles B, Price K. 2015. Simulating vegetation controls on hurricane-induced shallow landslides with a distributed ecohydrological model. *Journal of Geophysical Research: Biogeosciences* **120**(2): 361–378.

Jakob M, Bovis M, Oden M. 2005. The significance of channel recharge rates for estimating debris-flow magnitude and frequency. *Earth Surface Processes and Landforms* **30**: 755–766 https://doi.org/10.1002/esp.1188.

Karssenberg D, Schmitz O, Salamon P, de Jong K, Bierkens MFP. 2010. A software framework for construction of process-based stochastic spatio-temporal models and data assimilation. *Environmental Modelling and Software* **25**(4): 489–502 https://doi.org/10.1016/j.envsoft.2009.10.004.

Keim RF, Skaugset AE. 2003. Modelling effects of forest canopies on slope stability. *Hydrological Processes* **17**(7): 1457–1467.

Keijsers JGS, Schoorl JM, Chang KT, Chiang SH, Claessens L, Veldkamp A. 2011. Calibration and resolution effects on model performance for predicting shallow landslide locations in Taiwan. *Geomorphology* **133**(3-4): 168–177.

Kim JH, Fourcaud T, Jourdan C, Maeght JL, Mao Z, Metayer J, Meylan L, Pierret A, Rapidel B, Roupsard O, de Rouw A, Villatoro Sanchez M, Wang Y, Stokes A. 2017. Vegetation as a driver of temporal variations in slope stability: The impact of hydrological processes. *Geophysical Research Letters* **44**(10): 4897–4907.

Konnert V. 2004. Standortkarte Nationalpark Berchtesgaden. Forschungsbericht 49. ed. Nationalparkverwaltung Berchtesgaden.

Korup O, Densmore AL, Schlunegger F. 2010. The role of landslides in mountain range evolution. *Geomorphology* **120**(1-2): 77–90.

Kuriakose SL, Van Beek LPH, van Westen CJ. 2009. Parameterizing a physically based shallow landslide model in a data poor region. *Earth Surface Processes and Landforms* **34**(6): 867–881.

Liu S. 1997. A new model for the prediction of rainfall interception in forest canopies. *Ecological Modelling* **99**(2-3): 151–159.

Loacker H. 1971. Berg-und Grundwasserverhältnisse im Illgebiet. *Verhandlungen Geologische Bundesanstalt, Wien* **3**: 441–449.

Los SO, Pollack NH, Parris MT, Collatz GJ, Tucker CJ, Sellers PJ, Dazlich DA. 2000. A global 9-yr biophysical land surface dataset from NOAA AVHRR data. *Journal of Hydrometeorology* **1**(2): 183–199.

Malek Ž, Boerboom L, Glade T. 2015. Future Forest Cover Change Scenarios with Implications for Landslide Risk: An Example from Buzau Subcarpathians, Romania. *Journal of Environmental Management* **56**(5): 1228–1243. https://doi.org/10.1007/s00267-015-0577-y.

Malet JP, van Asch TW, Van Beek LPH, Maquaire O. 2005. Forecasting the behaviour of complex landslides with a spatially distributed hydrological model. *Natural Hazards and Earth System Science* **5**(1): 71–85.

Markart G, Perzl F, Kohl B, Luzian R, Kleemayr K, Ess B, Mayerl J. 2007. 22. und 23. August 2005 – Analyse von Hochwasser-und Rutschungsereignissen in ausgewählten Gemeinden Vorarlbergs. In: Schriftenreihe des Bundesforschungs- und Ausbildungszentrums für Wald, Naturgefahren und Landschaft 5.

Marquardt DW. 1969. An algorithm for least-squares estimation of nonlinear parameters. *Journal of the Society for Industrial and Applied Mathematics* **11**(2): 431–441.

Meng S, Jia Q, Zhou G, Zhou H, Liu Q, Yu J. 2018. Fine root biomass and its relationship with aboveground traits of Larix gmelinii trees in Northeastern China. *Forests* **9**(1): 35.

Meng W, Bogaard TA, Van Beek LPH. 2014. How the Stabilizing Effect of Vegetation on a Slope Changes Over Time: A Review. In *Landslide Science for a Safer Geoenvironment*, Sassa K, Canuti P, Yin Y (eds). Springer International Publishing: Cham; 363–372.

Mergili M, Fischer J-T, Krenn J, Pudasaini SP. 2017. r.avaflow v1, an advanced open source computational framework for the propagation and interaction of two-phase mass flows. *Geoscientific Model Development* **10**: 553–569 https://doi.org/10.5194/gmd-10-553-2017.

Mergili M, Marchesini I, Rossi M, Guzzetti F, Fellin W. 2014. Spatially distributed three-dimensional slope stability modelling in a raster GIS. *Geomorphology* **206**(1): 178–195 https://doi.org/10.1016/j.geomorph.2013.10.008.

Milledge DG, Bellugi D, McKean JA, Densmore AL, Dietrich WE. 2014. A multidimensional stability model for predicting shallow landslide size and shape across landscapes. *Journal of Geophysical Research: Earth Surface* **119**(11): 2481–2504.

Monteith JL. 1965. Evaporation and environment. *Symposia of the Society for Experimental Biology* **19**(205-23): 4.

Montgomery DR, Dietrich WE. 1994. A physically based model for the topographic control on shallow landsliding. *Water Resources Research* **30**(4): 1153–1171.

Montgomery RA, Chazdon RL. 2001. Forest structure, canopy architecture, and light transmittance in tropical wet forests. *Ecology* **82**(10): 2707–2718.

Oberhauser R. 1972. Geologisches Gutachten über das Gebiet des Walgaues nach Fragestellung der Raumplanung. Wien.

O'Loughlin C. 1974. The effect of timber removal on the stability of forest soils. *Journal of Hydrology (New Zealand)* **13**(2): 121–134.

Pack RT, Tarboton DG, Goodwin CN. 1998. *The SINMAP Approach to Terrain Stability Mapping, eighth congress of the International Association of Engineering Geology, Vancouver, British Columbia, Canada*. International Association of Engineering: Paris.

Papathoma-Köhle M, Glade T. 2013. The role of vegetation cover change for landslide hazard and risk. In *The Role of Ecosystems in Disaster Risk Reduction*, Renaud G, Sudmeier-Rieux K, Estrella M (eds). UNU-Press: Tokyo; 293–320.

Parameter Estimation Inc. 1999. *Model-Independent Parameter Estimation*. PEST Manual, Parameter Estimation Inc: Sandy.

Penman HL. 1948. Natural evaporation from open water, bare soil and grass. Proceedings of the Royal Society of London. A: Mathematical. *Physical and Engineering Sciences* **193**(1032): 120–145.

Promper C, Puissant A, Malet J, Glade T. 2014. Analysis of land cover changes in the past and the future as contribution to landslide risk Scenarios. *Applied Geography* **53**(1): 11–19.

Rodell M, Houser PR, Jambor U, Gottschalck J, Mitchell K, Meng C-J, Arsenault K, Cosgrove B, Radakovich J, Bosilovich M, Entin JK, Walker JP, Lohmann D, Toll D. 2004. The Global Land Data Assimilation System. *Bull. Amer. Meteor. Soc.* **85**(3): 381–394.

Rossi G, Catani F, Leoni L, Segoni S, Tofani V. 2013. HIRESSS: a physically based slope stability simulator for HPC applications. *Natural Hazards and Earth System Sciences* **13**(1): 151–166.

Rouse JW, Hass RH, Schell JA, Deering DW. 1973. Monitoring vegetation systems in the great plains with ERTS. *Third Earth Resour. Technol. Satell. Symp.* **1**: 309–317.

Ruff M, Czurda K. 2008. Landslide susceptibility analysis at a regional scale - A qualitative approach in the eastern alps. Intraprevent Conference Proceedings: 231-242.

Saxton KE, Rawls WJ. 2006. Soil water characteristic estimates by texture and organic matter for hydrologic solutions. *Soil Science Society of America Journal* **70**: 1569–1578.

Schmaltz EM, Steger S, Glade T. 2017. The influence of forest cover on landslide occurrence explored with spatio-temporal information. *Geomorphology* **290**(1): 250–264.

Schwarz M, Preti F, Giadrossich F, Lehmann P, Or D. 2010. Quantifying the role of vegetation in slope stability: a case study in Tuscany (Italy). *Ecological Engineering* **36**(3): 285–291.

Seijmonsbergen AC, de Jong MGG, de Graaff LWS, Anders NS. 2014. *Geodiversität von Vorarlberg und Liechtenstein-Geodiversity of Vorarlberg and Liechtenstein*. Haupt Verlag AG.

Seijmonsbergen AC. 1992. Geomorphological evolution of an alpine area and its application to geotechnical and natural hazard appraisal in the NW. Rätikon mountains and S. Walgau (Vorarlberg, Austria). Dissertation, University of Amsterdam: pp. 109.

Sellers PJ, Randall DA, Collatz GJ, Berry JA, Field CB, Dazlich DA, Bounoua L. 1996. A revised land surface parameterization (SiB2) for atmospheric GCMs. Part I: Model formulation. *Journal of Climate* **9**(4): 676–705.

Sidle RC, Bogaard TA. 2016. Dynamic earth system and ecological controls of rainfall-initiated landslides. *Earth-Science Reviews* **159**(1): 275–291.

Sidle RC, Ochiai H. 2006. *Landslides: processes, prediction, and land use*, Vol. **18**. American Geophysical Union: Washington DC.

Sidle RC, Pearce AJ, O'Loughlin CL. 1985. *Hillslope Stability and Land Use. American Geophysical Union. Water Resources Monograph*. D. C: Washington; 11.

Sidle RC, Ziegler AD, Negishi JN, Nik AR, Siew R, Turkelboom F. 2006. Erosion processes in steep terrain – truths, myths, and uncertainties related to forest management in Southeast Asia. *Forest Ecology and Management* **224**(1): 199–225.

Sidle RC, Ziegler AD. 2017. The canopy interception–landslide initiation conundrum: insight from a tropical secondary forest in northern Thailand. *Hydrology and Earth System Sciences* **21**: 651–667 https://doi.org/10.5194/hess-21-651-2017.

Sidle RC. 1992. A theoretical model of the effects of timber harvesting on slope stability. *Water Resources Research* **28**(7): 1897–1910.

Simoni S, Zanotti F, Bertoldi G, Rigon R. 2008. Modelling the probability of occurrence of shallow landslides and channelized debris flows using GEOtop-FS. *Hydrological Processes* **22**(4): 532–545.

Steger S, Schmaltz E, Seijmonsbergen AC, Glade T. 2018. The Walgau – a landscape shaped by landslides. In *Landscapes and Landforms of Austria, World Geomorphological Landscapes*, Embleton-Hamann C. (ed), Springer (accepted, print 2018): Heidelberg, New York.

Stewart JB. 1988. Modelling surface conductance of pine forest. *Agricultural and Forest Meteorology* **43**(1): 19–35.

Tarolli P, Tarboton DG. 2006. A new method for determination of most likely landslide initiation points and the evaluation of digital terrain model scale in terrain stability mapping. *Hydrology and Earth System Sciences* **10**(5): 663–677.

Tilch N. 2014. Identifizierung gravitativer Massenbewegungen mittels Multitemporaler Luftbildauswertung in Vorarlberg und angrenzender Gebiete. *Jahrbuch der Geologischen Bundesanstalt* **154**: 21–39.

Van Beek R. 2002. Assessment of the influence of changes in climate and land use on landslide activity in a Mediterranean environment. *Netherlands Geographical Studies* **294**: 366.

Vanacker V, Vanderschaeghe M, Govers G, Willems E, Poesen J, Deckers J, De Bievre B. 2003. Linking hydrological, infinite slope stability and land-use change models through GIS for assessing the impact of deforestation on slope stability in high Andean watersheds. *Geomorphology* **52**(3-4): 299–315.

Verstraeten WW, Muys B, Feyen J, Veroustraete F, Minnaert M, Meiresonne L, Schrijver AD. 2005. Comparative analysis of the actual evapotranspiration of Flemish forest and cropland, using the soil water balance model WAVE. *Hydrology and Earth System Sciences* **9**(3): 225–241.

Walach G, Weber F. 1977. Ein Beitrag zur Hydrogeologie des Walgaues auf Grund geophysikalischer Messungen. *Verb. Geol. B.-A.* **2**: 201–208.

Wartluft JL. 1978. Estimating top weights of hardwood sawtimber. In *Res. Pap. NE-427*, Vol. **7p**. US Department of Agriculture, Forest Service, Northeastern Forest Experiment Station: Broomall, PA; 427.

Watson A, Phillips C, Marden M. 1999. Root strength, growth, and rates of decay: root reinforcement changes of two tree species and their contribution to slope stability. *Plant and Soil* **217**(1): 39–47.

Wilson JB. 1988. A review of evidence on the control of shoot: Root ratio, in relation to models. *Annals of Botany* **61**: 433–449.

Wu Z, Wu J, Liu J, He B, Lei T, Wang Q. 2013. Increasing terrestrial vegetation activity of ecological restoration program in the Beijing–Tianjin sand source region of China. *Ecological Engineering* **52**: 37–50.

Zhou G, Meng S, Yu J, Zhou H, Liu Q. 2018. Quantitative relationships between fine roots and stand characteristics. *European Journal of Forest Research* **137**(3): 385–399.

Zieher T, Perzl F, Rössel M, Rutzinger M, Meißl G, Markart G, Geitner C. 2016. A multi-annual landslide inventory for the assessment of shallow landslide susceptibility – Two test cases in Vorarlberg. *Austria. Geomorphology* **259**(1): 40–54.

Ziemer RR. 1981. Roots and stability of forested slopes. – Erosion and sediment transport in Pacific Rim Steeplands. *IAHS* **132**: 343–361.

Zotarelli L, Dukes MD, Romero CC, Migliaccio KW, Morgan KT. 2010. Step by step calculation of the Penman-Monteith Evapotranspiration (FAO-56 Method). Institute of Food and Agricultural Sciences. University of Florida.

Supporting Information

Additional supporting information may be found online in the Supporting Information section at the end of the article.

Data S1: Supporting Information